J. Meas. Sci. Instrum., 2026, 17(1): 162-170.
DOI: 10.62756/jmsi.1674-8042.2026014
http://jmsi.publish.founderss.cn
jmsi@nuc.edu.cn

High-precision microcavity pressure sensing aided by MLP and GRNN

WANG Xiaohui[1,2], LI Wei[3*], WANG Canjin[4], LIU Wenyao[3*], TANG Jun[2*]

1. Department of Electronic Engineering, Taiyuan Institute of Technology, Taiyuan 030008, China;
2. School of Semiconductors and Physics, North University of China, Taiyuan 030051, China;
3. School of Instrument and Electronics, North University of China, Taiyuan 030051, China;
4. State Key Laboratory of Media Convergence Production Technology and Systems, Xinhua Zhiyun Technology Co., Ltd., Hangzhou 310030, China

***Corresponding author:** LI wei (liwei@nuc.edu.cn); TANG Jun (tangjun@nuc.edu.cn)

Received: December 1, 2025 **Revised:** January 9, 2026 **Accepted:** January 12, 2026

Abstract: In response to the requirements for high-precision detection and diverse data scenarios in the field of intelligent optical sensing, this research combines whispering gallery mode (WGM) microcavity sensing with machine learning to solve the problems of low spectral information utilization, large random errors, and poor adaptability to data scales in the traditional microcavity sensing. Firstly, the WGM microcavity sensing system is used to collect transmission spectral datasets of different scales. Secondly, a multi-layer perceptron (MLP) deep learning algorithm based on full-spectrum feature mapping is adopted to train and test the datasets through hierarchical feature extraction and nonlinear fitting. The results show that the MLP achieves the test accuracy of 99.95% on large datasets. However, it exhibits poor performance on small datasets. Subsequently, the generalized regression neural network (GRNN) is introduced, leveraging its non-iterative training and strong local feature fitting advantages to optimize the small sample scenarios. The results indicate that the GRNN can achieve a test accuracy of 98.85% on small data sample datasets, improving by 10.29% compared to MLP. Finally, this study quantitatively compares and analyzes the test performance of MLP and GRNN models for five datasets of different scales, clarifying the performance advantages of the two models under different data conditions. This study fully utilizes the characteristics of MLP and GRNN models to achieve high-precision detection under different data scales, providing strong technical support for the application of intelligent optical microcavity sensing technology in various scenarios.

Key words: machine learning; whispering gallery modes (WGM); microbottle resonant; pressure detection

0 Introduction

Whispering gallery modes (WGM) optical microcavities have become a promising sensing platform due to their high quality factor (Q value), miniaturized structure and superior optical performance. These microcavities can confine photons within a small mode volume for a long time, thereby significantly enhancing the interaction between light and matter, providing crucial support for the improvement of detection sensitivity and resolution[1]. Currently, WGM microcavities with various structures such as microrings, microdisks, micropillars, microspheres, and microbottles have become research hotspots[2-3]. Among them, the hollow microbottle resonantor (HMR) with a hollow structure has attracted much attention due to its excellent performance in the detection of liquid concentration, flow rate, and pressure[4-6].

Pressure is a basic physical parameter in chemistry, biology, physics and other disciplines, and its accurate measurement is of great significance. Traditional WGM microcavity pressure sensing mainly achieves detection by analyzing specific modes in the transmission spectrum, such as mode shift[7], mode broadening[8], and mode splitting[9]. However, manually selecting specific modes limits the accuracy of the sensor in three aspects. Firstly, the spectral information is not fully utilized. Only the characteristics of a single resonant mode are extracted, and the abundant pressure-related implicit information such as changes in the morphology of the spectrum, linewidth, and quality factor in the spectrum is not taken into account, resulting in low sensing accuracy. Secondly, human intervention introduces errors, making it difficult to meet the high-precision requirements. Thirdly, it has poor adaptability to data scale and environmental interference. When the pressure gradient is sparse (in small sample scenarios) or there are interferences of temperature drifts and vibrations, a single mode analysis is prone to misjudgment, which also leads to a significant drop in detection accuracy. These limitations are difficult to be resolved through hardware structure optimization alone. However, machine learning technology has the capabilities of full feature mining, nonlinear fitting, and adaptive modeling, which can intelligently interpret the complete spectral information, avoid human intervention errors, and adapt to different data scales[10-12].

In recent years, with the development of artificial intelligence, machine learning technology has been widely applied in the field of optical microcavity sensing, especially showing significant advantages in multi-modal data processing[13-14]. For instance, Duan et al. [15] constructed a pressure detection system based on microsphere resonators, using the multilayer perceptron (MLP) deep learning algorithm to analyze all features of the spectrum, and finally achieved a pressure test accuracy of 99.97%. Compared with the traditional method of extracting a single resonant mode for analysis, the measurement accuracy is improved by 11.5%. Chen et al.[16] studied the temperature sensing of microsphere resonators based on the generalized regression neural network (GRNN), achieving both high accuracy and a large dynamic range. Within the range of 25.00 ℃ to 40.00 ℃, the detection accuracy reached 3.8×10^{-3} ℃. In our previous research[17], it has also been confirmed that the ethanol concentration sensor based on MLP for full-spectrum analysis has a testing accuracy that is 13.02% higher than that of the sensor that only extracts a few local features. However, most of the existing research focuses on the application of a single machine learning algorithm and has not yet conducted algorithm adaptability studies for different data scale fields.

Therefore, based on the previous research, the MLP and GRNN models are applied to WGM microcavity pressure sensing to analyze the difference test performance under different scale data. Finally, high-precision intelligent microcavity pressure sensing is realized to adapt to different scale datasets. The specific research process is as follows: Firstly, a WGM microbottle resonant cavity pressure detection system is designed, combined with the study of the influence of microcavity wall thickness on pressure sensitivity, and a high-sensitivity pressure sensing unit is prepared. Subsequently, spectral data are collected at different pressure setting points, and divided into non-overlapping training and testing datasets, which are used for model training and performance evaluation, respectively. Finally, the test performance of MLP and GRNN on different scale datasets is compared and analyzed. The experimental results show that when the data samples are sufficient, both the MLP and GRNN models exhibit excellent sensing performance; however, when only a sparse dataset with only six different pressure gradients is used, the test accuracy of MLP and GRNN is 88.56% and 98.85%, respectively. Obviously, compared with the MLP algorithm, the GRNN has better performance in small sample measurement scenarios.

1 Sensing principle and algorithm

1.1 Sensing principle

As shown in Fig. 1, when the laser is introduced into the optical tapered fiber, the light that satisfies the total internal reflection condition will be totally reflected on the surface of the HMR. When the optical path traveled by the light in the microcavity is equal to an integer multiple of the wavelength, the optical field will form a stable resonant mode. For WGM microcavities, their resonant conditions can be expressed as [18]

$$\lambda=\frac{2\pi rn}{m}, \tag{1}$$

where λ is the resonant wavelength, r is the microcavity radius, n is the effective refractive index of WGM, and m is the number of azimuth modes.

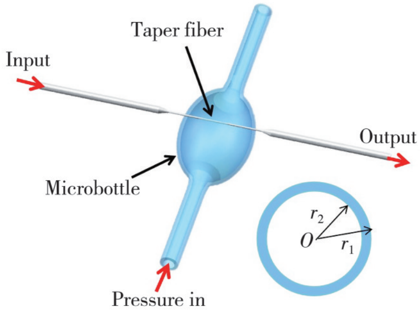

Fig. 1 HMR and tapered fiber coupling structure (inset is cross-sectional view of HMR)

The core working principle of WGM microcavity pressure sensing is to detect the shift of the WGM resonance wavelength. Initially, the microcavity is in a balanced state, producing a stable transmission spectrum, and the corresponding resonant wavelength remains constant. When different pressures are applied to the HMR, the size and effective refractive index of the microcavity will be changed, ultimately causing a shift in WGM resonance wavelength [18]. The total displacement generated by the resonant wavelength λ can be expressed as[19-22]

$$\frac{\mathrm{d}\lambda}{\lambda}=\frac{\mathrm{d}r}{r}+\frac{\mathrm{d}n}{n}. \tag{2}$$

In the following, we will approximate the HMR as a thin spherical glass shell, r_1 and r_2 represent the outer and inner radii of the HMR, p_{in} and p_{ex} represent the internal and external pressures of the HMR, and n_0 represents the refractive index of the HMR, respectively. The pressure expansion of HMR is calculated at $r=r_1$, and the strain term is further derived as function of p_{in}[22].

$$\frac{\mathrm{d}r(p_{\mathrm{in}})}{r_1}=\frac{(4G+3K)p_{\mathrm{in}}r_2{}^3-4Gp_{\mathrm{ex}}r_1{}^3-3Kp_{\mathrm{ex}}r_2{}^3}{12GK(r_1{}^3-r_2{}^3)}, \tag{3}$$

where the shear modulus and bulk modulus are $G=31\times10^9$ Pa and $K=41\times10^9$ Pa, respectively. The pressure dependency of the refractive index can be calculated from the Maxwell-Neumann equation by using the normal stress distributions as[22]

$$\frac{\mathrm{d}n}{n}=\frac{3(p_{\mathrm{in}}r_2{}^3-p_{\mathrm{ex}}r_1{}^3)C}{n_0(r_1{}^3-r_2{}^3)}. \tag{4}$$

The silica birefringence constant $C=4\times10^{-12}\,\mathrm{m}^2/\mathrm{N}$. From Eqs. (2) — (4), it can be seen that the resonant wavelength moves linearly with the internal pressure p_{in}. Then, the internal pressure sensitivity S_{p} of the HMR is

$$S_{\mathrm{p}}=\frac{\mathrm{d}\lambda}{\mathrm{d}p}=\left(\frac{4G+3K}{12GK}+\frac{3C}{n_0}\right)\chi, \tag{5}$$

where the geometric parameter χ represents

$$\chi=\frac{r_2^3}{r_1^3-r_2^3}. \tag{6}$$

Therefore, the thickness of the microcavity wall is a key factor affecting the internal pressure sensitivity of the HMR. The larger the volume of the microcavity, the thinner the wall thickness, and the higher the pressure sensing sensitivity. Based on this, subsequent experiments will compare and analyze the sensing sensitivity of two microcavities with different wall thicknesses.

1.2 MLP algorithm

The MLP model consists of three layers of neurons: an input layer, a hidden layer and an output layer. The input layer receives the transmission spectral characteristics corresponding to different pressures, which are input in the form of a matrix; the output layer exports the pressure value corresponding to the transmission spectrum; and the hidden layer is used to adjust the nonlinear relationship between the input layer and the output layer[15]. Its structure is shown in Fig. 2(b), and each neuron between layers is connected through weights, forming a fully connected layer. For a single hidden layer model, the relationship between the output y and the input x_{i} is[25]

$$y=\sum_{i=1}^{m}\omega_i f\left(b_0+\sum_{j=1}^{n}x_i\omega_{ij}\right), \tag{7}$$

where b_0 is the bias term, w_i and w_{ij} are the weight factors of the input layer and the output layer respectively, x_{i} represents the ith pressure value, and $f(\bullet)$ is a nonlinear activation function. The activation function used in this study is the ReLU function.

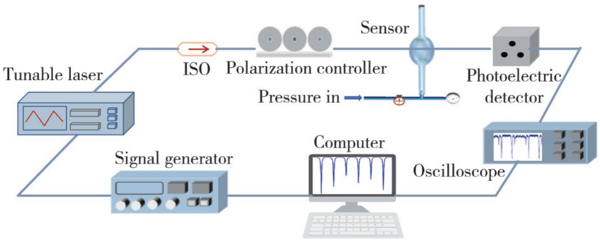

(a) pressure detection system

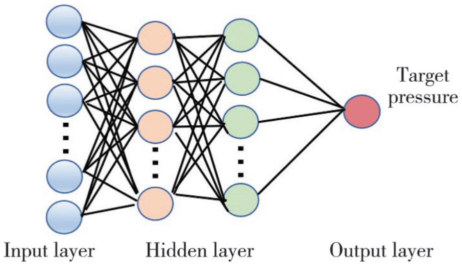

(b) MLP model

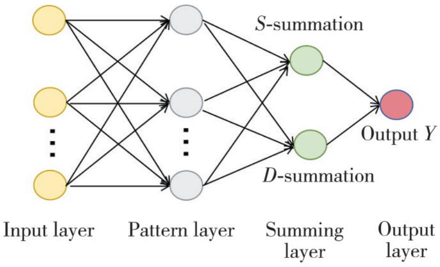

(c) GRNN model

Fig. 2 Schematic diagram of sensor system design

The construction of the MLP includes two processes: training and testing processes. Among them, the core purpose of the training process is to adjust the biases and weight factors of the input and output layers through the loss function until the model generates the optimal target output, thereby obtaining a stable and highly performing model. The testing process is to verify the performance of the model using the data that are not participated in the training. After the model training is completed, the test data are input into the model to evaluate the test accuracy of the model. In this process, the mean squared error (MSE) can be used for assessment, defined as[26]

$$\sigma_{\mathrm{MSE}}=\frac{1}{N}\sum_{i=1}^{N}(p_i-\hat{p}_i)^2. \tag{8}$$

In addition, the coefficient of determination (R^2) can also be used to quantify the final test accuracy, which is defined as[15]

$$R^2 = 1 - \frac{\sum_{i=1}^{N}(\hat{p}_i - p_i)^2}{\sum_{i=1}^{N}(\bar{p} - p_i)^2}, \tag{9}$$

where p_i and $\hat{p}_i$ represent the true value of the ith sample and the network test value, respectively; $\bar{p}$ is the average of the true values; and N is the total number of test samples.

1.3 GRNN algorithm

Different from the iterative training mechanism of MLP, GRNN directly constructs the function mapping relationship between the input and output from the training data, which has potential advantages for analyzing small sample datasets. As shown in Fig.2(c), the basic structure of GRNN consists of four parts: the input layer, the pattern layer, the summing layer, and the output layer. Among them, the pattern layer uses the Gaussian function as the activation function, and calculates the Euclidean distance between the input vector and the training sample by adjusting the smoothing factor σ, thereby achieving the nonlinear mapping of the input data. Its mathematical expression is[28]

$$\varphi(\|\boldsymbol{x} - \boldsymbol{p}_i\|) = \exp\left(-\frac{\|\boldsymbol{x} - \boldsymbol{p}_i\|^2}{2\sigma^2}\right), \tag{10}$$

where $\boldsymbol{x}$ is the input data vector, $\boldsymbol{p}_{\mathrm{i}}$ is the center point corresponding to the ith pattern layer neuron, σ is the smoothing factor, and $\|\cdot\|$ represents the Euclidean distance. According to Eq. (10), when the input $\boldsymbol{x}$ is close to the center point $\boldsymbol{p}_i$, the function value is larger; as the distance between $\boldsymbol{x}$ and $\boldsymbol{p}_i$ increases, the function value rapidly decays and approaches 0. The summation layer contains two sub-layers: the weighted summation layer (S-summation neurons) and the arithmetic summation layer (D-summation neurons). Among them, the S-summation neurons are used to calculate the weighted sum of the output of the pattern layer, while the D-summation neurons are used to calculate the unweighted sum of the output of the pattern layer. The operation relationship is[28]

$$S = \sum_{i=1}^{n} Y_{\mathrm{i}} \exp\left(-\frac{(\boldsymbol{X} - \boldsymbol{X}_i)^{\mathrm{T}}(\boldsymbol{X} - \boldsymbol{X}_i)}{2\sigma^2}\right), \tag{11}$$

$$D = \sum_{i=1}^{n} \exp\left(-\frac{(\boldsymbol{X} - \boldsymbol{X}_i)^{\mathrm{T}}(\boldsymbol{X} - \boldsymbol{X}_i)}{2\sigma^2}\right), \tag{12}$$

where Y_i represents the weight from the ith neuron in the connection mode layer to the summing layer, X_i represents the input vector of the ith training sample, and $\boldsymbol{X}$ is the number of samples to be tested. For the input vector $\boldsymbol{X}$, the output Y of the GRNN is the ratio of the result of the weighted summing layer to the result of the arithmetic summation layer. The purpose is to ensure that the output value is the weighted average of all training samples, and its expression is

$$Y(X) = \frac{S}{D} = \frac{\sum_{i=1}^{n} Y_i \exp\left(-\frac{(\boldsymbol{X} - \boldsymbol{X}_i)^{\mathrm{T}}(\boldsymbol{X} - \boldsymbol{X}_i)}{2\sigma^2}\right)}{\sum_{i=1}^{n} \exp\left(-\frac{(\boldsymbol{X} - \boldsymbol{X}_i)^{\mathrm{T}}(\boldsymbol{X} - \boldsymbol{X}_i)}{2\sigma^2}\right)}. \tag{13}$$

In this research, the final test results are evaluated by using the MSE and R^2. The smaller the MSE, the smaller the deviation between the predicted value of the model and the true value; the larger the R^2 value, the higher the fitting degree of the model to the test data, that is, the better the test performance of the model.

2 Experimental setup and results

2.1 Construction of sensing system

The data acquisition system of the WGM microcavity pressure sensor is achieved through the coupling of the tapered fiber and the HMR. The HMR is prepared from silica capillary tubes. The preparation process is as follows: First, connect one end of the capillary tube to a pressure pump, and use an optical fiber fusion splicer (S183PM) to discharge and fuse the other end to make it sealed; then, move the precise position of the capillary structure to be prepared between the two electrodes of the fusion splicer and adjust the discharge time and current; finally, the capillary is pressurized from one end connected to the pressure pump and then discharged. Under the action of air pressure, the partially discharged and heated part of the capillary tube gradually expands to form the desired capillary shape. During the preparation process, the part of the capillary heated by discharge gradually expands to form the required microbottle shape. During the preparation process, the wall thickness of the HMR is mainly controlled by regulating the air pressure, discharge time and number of discharges. To verify the influence of different wall thicknesses on the sensitivity of pressure detection, two HMRs with wall thicknesses of approximately 8.6 μm and 14.3 μm are prepared at different positions of the same capillary tube. During pressure detection, to prevent gas leakage, the sealed end of the capillary tube is re-sealed with ultraviolet (UV) glue. Additionally, the tapered fiber is fabricated from single-mode optical fibers (with a core diameter inner diameter of 8.3 μm and an outer diameter of

125 μm) through hydrogen-oxygen flame heating. By adjusting the flame position and stretching rate, different diameters of tapered bodies can be obtained. This process can be monitored in real time in the CCD imaging system to detect the changes in the fiber size. In the experiment, a tapered optical fiber with a diameter of approximately 2.3 μm that matches the HMR is prepared. The preparation processes of the HMR and the tapered optical fiber have been described in detail in our previous studies[17,23].

To reduce the noise interference caused by external environmental and enhance the stability of the coupling system, the sensing unit is packaged in this study. The specific packaging process is described in detail in our previous studies[17,23]. The encapsulated sensing system is placed in an acrylic box, which further improves the robustness and anti-interference ability of the system, ensuring its stable and accurate operation in complex application scenarios, and providing a more reliable guarantee for subsequent experiments and practical applications.

The principle of the WGM microbottle resonator pressure detection system is shown in Fig. 2(a). This system consists of an optical transmission system, a pressure transmission system, and a display system. Among them, the optical transmission system is composed of a tunable laser (1 550 nm, NKT Company), an isolator, a polarization controller (PC), and a packaged sensor; the pressure transmission system changes the internal pressure value of the microcavity through a pressure pump, and displays the actual pressure value through a pressure gauge; the display system is composed of an oscilloscope and a computer, and the computer will automatically collects data at the set time intervals to conduct in-depth data analysis and processing for the subsequent machine learning. In addition, a function generator is used to generate a triangular wave modulation signal with a peak-to-peak value of 10 V, which is connected to the laser to achieve linear continuous scanning of the laser frequency. During the experiment, the packaged sensor is placed on an isolation platform, and the laboratory temperature is controlled to be 25 ℃ with a relative humidity of 30% to minimize the interference of the external environment on the experimental results.

Fig.3(a) shows the WGM transmission spectrum corresponding to a pressure value of 10 kPa, and it can be seen that there are multiple modes in the transmission spectrum. Usually, the typical resonant peak with a high quality factor (Q) is selected to achieve sensing. The Q values of the resonant peaks Tip1 and Tip2 obtained by Lorentz fitting are 3.6×10^7 and 6.8×10^6, respectively, as shown in Fig.3(b). Next, the experimental device is used to conduct pressure sensitivity tests on HMRs with two different wall thicknesses.

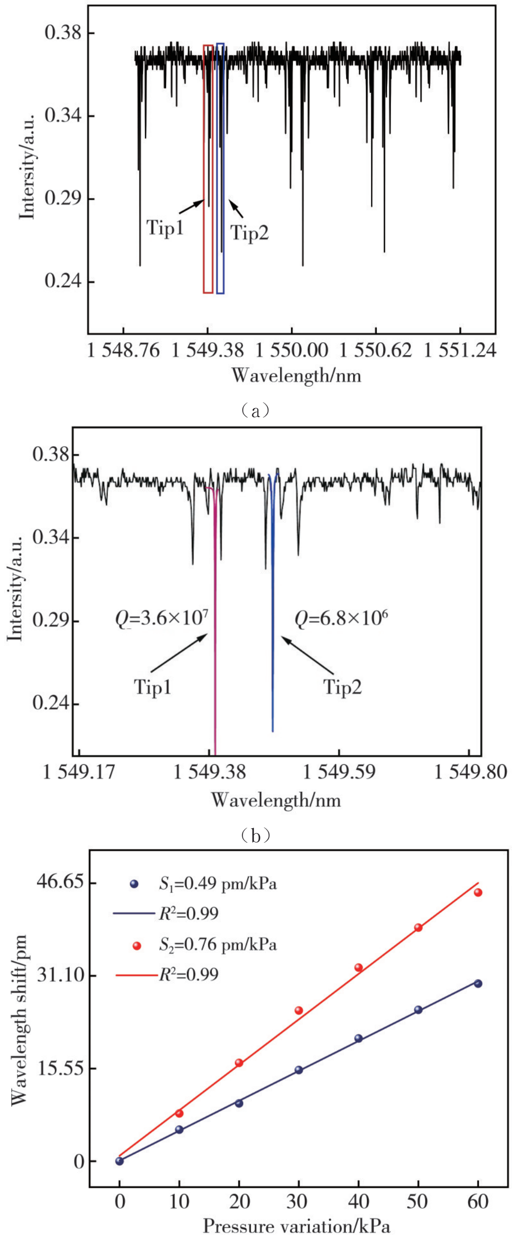

(a)

(b)

(c)

Fig. 3 Traditional HMR pressure sensing. (a) Transmission spectrum of the sensor at a specific pressure, (b) Fitted Lorentz curve, and (c) Linear fitting between different pressures and wavelength shift with different wall thickness

During the experiment, the pressure is manually adjusted through the pressure regulator, and the applied pressure values are recorded using the calibrated electronic pressure sensor. The results show that as the internal pressure of the HMR increases, the resonance wavelength of the transmitted light spectrum to shift towards the red.

Fig.3(c) shows the pressure sensing characteristics of the HMR with two wall thicknesses. Through linear fitting, it is indicated that the pressure sensing sensitivity with a wall thickness of 14.3 μm and 8.6 μm is 0.49 pm/kPa and

0.76 pm/kPa, respectively. This result proves that the pressure sensing sensitivity of thin-walled HMR has been significantly improved. However, it should be noted that as the wall thickness of the HMR continues to decrease, its mechanical strength will also significantly decrease, leading to the sensor being prone to damage. Therefore, the wall thickness of HMR needs to be reasonably balanced among sensitivity, mechanical stability, and measurement range.

2.2 Sensor performance analysis assisted by MLP

Based on the above experiments, thinner-walled sensing unit is selected for pressure data acquisition, and the pressure test data are intelligently processed using the MLP deep learning algorithm firstly.

In the data collection process, it is necessary to wait for the spectrum to stabilize before collecting data after the pressure value changes. Based our previous research of WGM sensor stability[17,23], the data collection starts 20 s after the pressure adjustment in this study. For the spectral data corresponding to a single pressure, the system automatically collects a set of data every 9 s, and a total of 33 sets of data are obtained for 5 min of continuous collection. Based on this, the experiment constructs a small dataset under six different pressure gradients and a large dataset under 30 different pressure gradient. Before training, the datasets are randomly divided into a training set and a test set at a ratio of 80% and 20%. Subsequently, the MLP prediction model is optimized through parameter optimization.

In our work, we mainly investigate the impact of different-sized datasets on the performance of the MLP model. Based on our previous research[17], when the number of hidden layers is too large, it will lead to the problem of over-fitting. Therefore, a single hidden layer structure is used to build the model. The learning rate adjustment adopts an adaptive learning rate optimization to the optimal learning rate. The study focuses on analyzing the effects of two key parameters, the epochs and the number of neurons in the hidden layer, on the fitting effect and generalization ability of the model.

The results in Fig.4 (a) and 4 (d) show the influence of the epochs on the MSE under two different scale datasets, respectively. The results indicate that for the small datasets, after the training epochs exceed 500, the MSE value fluctuates significantly and the MSE is relatively large. This is because the sparse data samples make it difficult for the MLP model to converge, thereby affecting the stability of the model. The Fig.4 (b) and 4 (e) show the influence of the number of neurons in the single hidden layer on MSE under two scale datasets, respectively. The results further indicate that the sparse dataset affects the stability of the MLP model. The final test results show that for the small datasets, the test accuracy R^2 of the MLP model is 88.56%, as shown in Fig. 4 (c); however, for the large dataset, its test accuracy is 99.95%, as shown in Fig.4 (f).

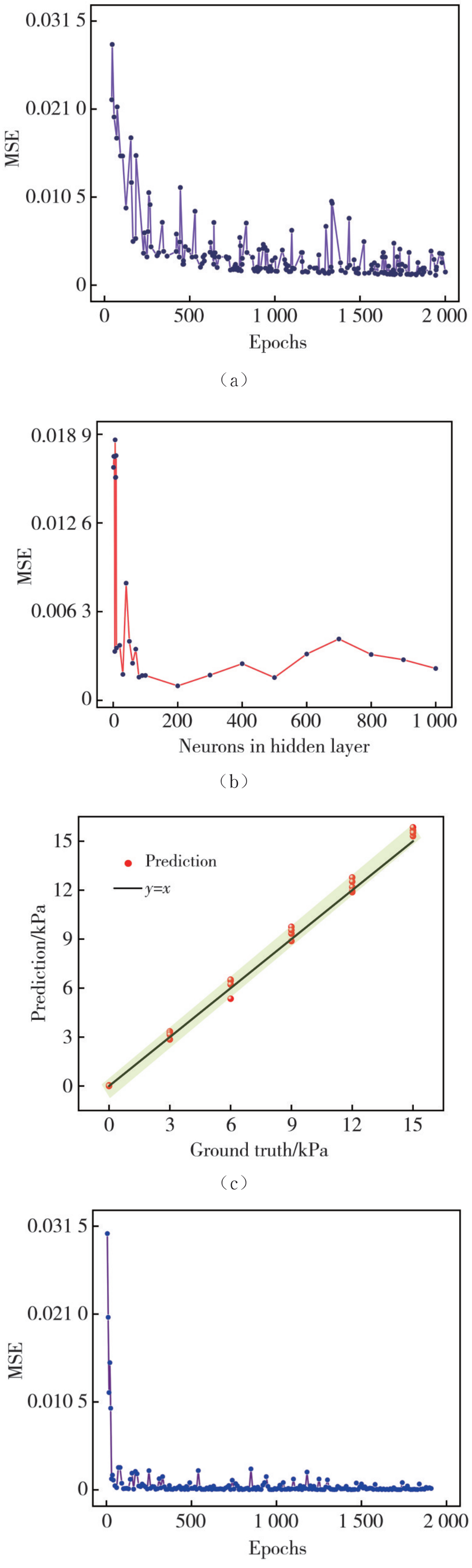

(a)

(b)

(c)

(d)

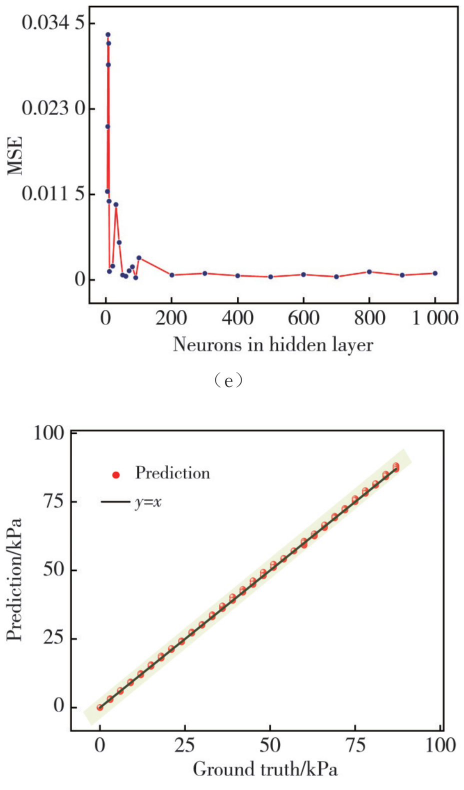

(e)

(f)

Fig. 4 Optimization of MLP model parameters. (a–c) Six different pressure gradient data samples: (a) relationship between epochs and MSE, (b) relationship between the number of neurons in hidden layer and MSE, and (c) comparison of ground truth and prediction values based on MLP; (d–f) 30 different pressure gradient data samples: (d) relationship between epochs and MSE, (e) relationship between the number of neurons in hidden layer and MSE, and (f) comparison of ground truth and prediction values based on MLP

Thus, it can be seen that the performance of the MLP model is related to the size of the data sample. Sufficient sample size can improve the stability and testing accuracy of the model.

2.3 Sensor performance analysis assisted by GRNN

Regarding the problem that the MLP model has a large MSE when testing small data samples, this study introduces GRNN[27] for performance optimization and comparative analysis. Next, the same small data samples (containing only six different pressure gradient spectral data) are divided into 80% ratio and input into the GRNN network for training. By adjusting the smoothing factor σ, the results show that when the value of σ is set to 0.05, the model achieved the minimum MSE, as shown in Fig. 5(a). The remaining 20% sample set are used to test the model, the relationship between the true pressure values and the test values is obtained, with an R^2 value of 98.85%, as shown in Fig. 5(b). Compared to the MLP model, the test accuracy increased by 10.29%.

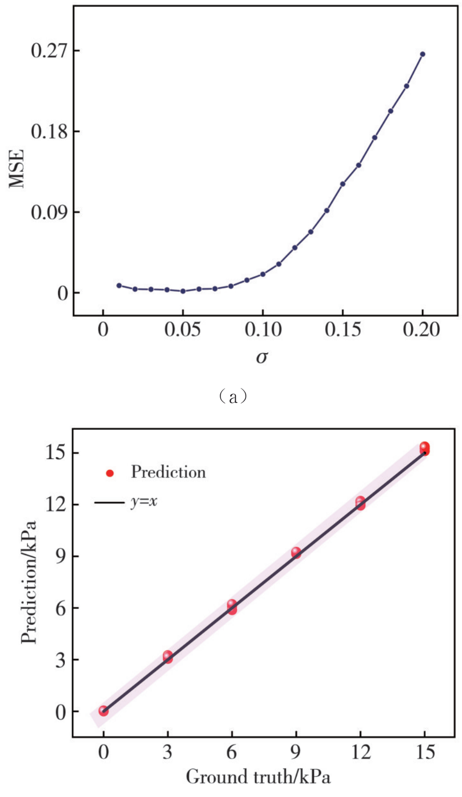

(a)

(b)

Fig. 5 Performance analysis of GRNN Model. (a) Relationship between the smoothing factor and MSE, and (b) Comparison of true and prediction values based on GRNN with small-data sample

Finally, the large dataset sample containing 30 spectra under different gradient pressures is divided into sub-datasets with 6, 12, 18, 24, and 30 pressure gradients, respectively. These sub-datasets are applied to the training and testing of the MLP and GRNN models, and the performances are compared and analyzed. As shown in Fig. 6 the smaller the data sample, the more significant the superior performance of the GRNN model. Specifically, for the sparse sample dataset containing 6 pressure gradients, the test accuracy of the GRNN model is 10.29% higher than that of the MLP model; for the dataset containing 12 pressure gradients, the test accuracy of the GRNN model is 9.03% higher than that of the MLP model; while in the case of sufficient data samples, the test accuracy of the GRNN and MLP models is 99.38% and 99.95% respectively, and their performances are comparable. It should be noted that the R^2 is the average value obtained after each model has been tested 10 times to ensure the stability and reliability of the results.

It can be seen that GRNN, with its non-iterative training, strong local feature fitting and fast convergence characteristics, demonstrates excellent generalization ability when dealing with sparse sample datasets. This is mainly attributed to the complex training process of MLP and its tendency to get stuck in local optimal solutions. In contrast, GRNN constructs the model by directly using the center points of the training data, enabling rapid convergence and thus providing accurate test results. Therefore, in the application of WGM microcavity sensing, MLP and GRNN each have their own advantages. MLP has strong generalization ability and wide applicability; GRNN has more advantages in processing sparse data sample scenarios. Therefore, we can decide to use MLP or GRNN based on specific application requirements and data characteristics.

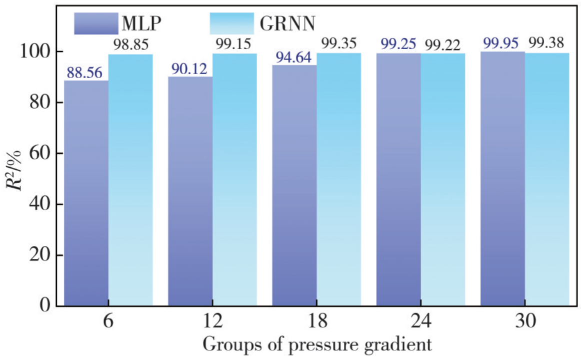

Fig. 6 Comparison of test performance between MLP and GRNN models

3 Conclusions

This paper introduces two deep learning algorithms, MLP and GRNN, to test and conduct comparative analysis on different scale datasets collected by traditional WGM microcavity pressure sensing. The experimental results show that when only using a small dataset under six different pressure gradients, the test R^2 value of the MLP model is 88.56%; while when the dataset is expanded to 30 different pressure gradients, its test R^2 value is 99.95%. However, when the above small data samples are used for the GRNN model, its R^2 value can reach 98.85%, which is 10.29% higher than that of the MLP model. Through comparative analysis, it can be concluded that for sparse sample data, the R^2 value of the GRNN model is higher than that of the MLP model, and its test performance is better. While in the case of sufficient data samples, the test effects of both models are comparable. Therefore, in practical applications, the appropriate model can be selected based on specific requirements and data characteristics to provide a reference for diverse application scenarios.

Acknowledgement

This work was supported by Talent Recruitment and Research Funding Program of Taiyuan Institute of Technology (No.2025KJ031).

Declaration of conflicting interests

The authors have no conflict of interests related to this publication.

References

[1] GRUDININ I S, MATSKO A B, MALEKI L. Brillouin lasing with a CaF_2 whispering gallery mode resonator. Physical Review Letters, 2009, 102(4): 043902.

[2] Huang jiaqi, Zouhui, Research progress of whispering gallery mode optical microcavity and its application. Study on Optical Communication, 2024, 50(3): 23003901-23003909.

[3] PAN Z W, YANG Y, LIU W Y, et al. Ultra-stable phonon laser through closed-loop feedback control for optomechanical sensing. Laser & Photonics Reviews, 2024, 18(12): 2400593.

[4] TANG S J, LI B B, , XIAO Y F. Optical sensing with whispering-gallery microcavities. Physics, 2019, 48(3): 137-147.

[5] MEMON S F, WANG R N, STRUNZ B, et al. A review of optical fibre ethanol sensors: current state and future prospects. Sensors, 2022, 22(3): 950.

[6] SU X D, SUTARLIE L, LOH X J. Sensors, biosensors, and analytical technologies for aquaculture water quality. Research, 2020: 8272705.

[7] ZHU H Y, WHITE I M, SUTER J D, et al. Analysis of biomolecule detection with optofluidic ring resonator sensors. Optics Express, 2007, 15(15): 9139-9146.

[8] FOREMAN M R, SWAIM J D, VOLLMER F. Whispering gallery mode sensors. Advances in Optics and Photonics, 2015, 7(2): 168.

[9] SMITH D D, CHANG H, FULLER K A. Whispering-gallery mode splitting in coupled microresonators. Journal of the Optical Society of America B, 2003, 20(9): 1967.

[10] YANG Y, SAURABH S, WARD J M, et al. High-Q, ultrathin-walled microbubble resonator for aerostatic pressure sensing. Optics Express, 2016, 24(1): 294-299.

[11] ZHANG Y N, ZHOU T M, HAN B, et al. Optical bio-chemical sensors based on whispering gallery mode resonators. Nanoscale, 2018, 10(29): 13832-13856.

[12] JORDAN M I, MITCHELL T M. Machine learning: Trends, perspectives, and prospects. Science, 2015, 349 (6245): 255-260.

[13] XIE Y X, WU X H, HUANG X B, et al. A deep learning-enabled skin-inspired pressure sensor for complicated recognition tasks with ultralong life. Research, 2023, 6: 0157.

[14] CHEN Q W, CHEN L X, FU Z X, et al. Optical frequency comb-based aerostatic micro pressure sensor aided by machine learning. IEEE Sensors Journal, 2023, 23(18): 21078-21083.

[15] DUAN B, ZOU H Y, CHEN J H, et al. High-precision whispering gallery microsensors with ergodic spectra empowered by machine learning. Photonics Research, 2022, 10(10): 2343.

[16] CHEN H, WANG Z Y, WANG Y, et al. Machine learning-assisted high-accuracy and large dynamic range thermometer in high-Q microbubble resonators. Optics Express, 2023, 31(10): 16781-16794.

[17] WANG X H, LIU W Y, CHEN H Y, et al. High-precision ethanol concentration microsensor with global spectra aided by the multi-layer perceptron. Optics Express, 2024, 32(24): 42983.

[18] ZHI Y Y, YU X C, GONG Q H, et al. Single nanoparticle detection using optical microcavities. Advanced Materials, 2017, 29(12): 1604920.

[19] LU Q J, LIAO J, LIU S, et al. Precise measurement of micro bubble resonator thickness by internal aerostatic pressure sensing. Optics Express, 2016, 24(18): 20855-20861.

[20] YANG Y, SAURABH S, WARD J, et al. Coupled-mode-induced transparency in aerostatically tuned microbubble whispering-gallery resonators. Optics Letters, 2015, 40(8): 1834.

[21] IOPPOLO T, ÖTÜGEN M V. Pressure tuning of whispering gallery mode resonators. Journal of the Optical Society of America B, 2007, 24(10): 2721.

[22] HENZE R, SEIFERT T, WARD J, et al. Tuning whispering gallery modes using internal aerostatic pressure. Optics Letters, 2011, 36(23): 4536-4538.

[23] WANG X H, LIU W Y, CHEN H Y, et al. Trace ethanol concentration sensor based on hollow microbubble resonator modified with $MnCo_2O_{4.5}$. IEEE Sensors Journal, 2024, 24(3): 2396-2404.

[24] WU Y R, DUAN B, LI C H, et al. Multimode sensing based on optical microcavities. Frontiers of Optoelectronics, 2023, 16(1): 29.

[25] LECUN Y, BENGIO Y, HINTON G. Deep learning. Nature, 2015, 521(7553): 436-444.

[26] NICOLSON A, PALIWAL K K. Deep learning for minimum mean-square error approaches to speech enhancement. Speech Communication, 2019, 111(8): 44-55.

[27] IZONIN I, KRYVINSKA N, TKACHENKO R, et al. An extended-input GRNN and its application. Procedia Computer Science, 2019, 160: 578-583.

[28] LÁZARO J, ARIAS J, ASTARLOA A, et al. Hardware architecture for a general regression neural network coprocessor. Neurocomputing, 2007, 71(1/2/3): 78-87.

MLP和GRNN辅助的微腔高精度压力传感

王晓慧[1,2], 李　伟[3*], 王灿进[4], 刘文耀[3], 唐　军[2]

1. 太原工业学院 电子工程系, 山西 太原 030008;
2. 中北大学 半导体与物理学院, 山西 太原 030051;
3. 中北大学 仪器与电子学院, 山西 太原 030051;
4. 新华智云科技有限公司 媒体融合生产技术与系统国家重点实验室, 浙江 杭州 310030

摘　要: 为满足智能光学传感领域对高精度检测及多样化数据场景的适配要求, 本研究将回音壁模式(Whispering gallery mode, WGM)微腔传感与机器学习结合, 以解决传统微腔传感中低频谱信息利用率低、随机误差大以及对数据规模适应性差等问题。首先, 通过WGM微腔传感系统采集不同规模的透射光谱数据集; 其次, 采用基于全光谱特征映射的多层感知机(Multilayer Perceptron, MLP)深度学习算法, 经层级化特征提取与非线性拟合对数据集进行训练与测试。结果显示, MLP模型在大数据集上的测试精度能达到99.95%, 但在小数据集上性能欠佳。随后, 引入广义回归神经网络(Generalized regression neural network, GRNN), 利用其非迭代训练与局部特征强拟合优势优化小样本场景。结果表明, GRNN对小数据样本集的测试精度可达98.85%, 较MLP提升了10.29%。最后, 本研究针对5种不同规模的数据集, 定量对比分析了MLP与GRNN模型的测试性能, 明确了两种模型在不同数据条件下的性能优势。本研究充分利用了MLP和GRNN模型的特点, 在不同数据规模下实现了高精度检测, 为智能光学微腔传感技术在多样化场景中的应用提供了有力技术支撑。

关键词: 机器学习; 回音壁模式; 微瓶谐振腔; 压力检测

引用格式: WANG Xiaohui, LI Wei, WANG Canjin, et al. High-precision microcavity pressure sensing aided by MLP and GRNN. Journal of Measurement Science and Instrumentation, 2026, 17(1): 162-170. DOI: 10.62756/jmsi.1674-8042.2026014